Inorg. Chem. **2006**, *45*, 2661–2668

Fiber-Optic Infrared Spectroelectrochemical Studies of Six-Coordinate Manganese Nitrosyl Porphyrins in Nonaqueous Media

Zaki N. Zahran,[†] Michael J. Shaw,[‡] Masood A. Khan,[†] and George B. Richter-Addo*,[†]

Department of Chemistry and Biochemistry, University of Oklahoma, 620 Parrington Oval, Norman, Oklahoma 73019, and Department of Chemistry, Box 1652, Southern Illinois University, Edwardsville, Edwardsville, Illinois 62026

Received July 15, 2005

The redox behavior of the six-coordinate (por)Mn(NO)(1-MeIm) (por = tetraphenylporphyrin dianion (TPP), tetratolylporphyrin dianion (TTP), or tetra-*p*-methoxyphenylporphyrin dianion (T(*p*-OMe)PP)) complexes were examined by cyclic voltammetry at room temperature and at –78 °C in two nonaqueous solvents (CH_2Cl_2 and THF) at a Pt disk electrode. In CH_2Cl_2 at room temperature, the compounds undergo four oxidations and two reductions within the solvent limit; in THF, the compounds undergo one oxidation and three reductions. In both solvents, the first oxidation represents a chemically irreversible one-electron process involving the rapid loss of nitric oxide. The oxidation occurs at the MnNO site as judged from bulk electrolysis, UV–vis spectroscopy at room temperature, and IR spectroelectrochemistry at room temperature and at –78 °C. The second oxidation, accessible in CH_2Cl_2, is also chemically irreversible and occurs at the porphyrin ring; the third and the fourth oxidations are, on the other hand, chemically reversible but also occur at the porphyrin ring**.** The first reduction is chemically irreversible in CH_2Cl_2, occurs at the porphyrin ring, and is followed by loss of NO. In THF, the first reduction is chemically reversible and is followed by reversible loss of NO.

Introduction

Nitric oxide (NO) interacts with many heme proteins in vivo and in vitro, and many of these interactions that result in Fe−NO bonds are physiologically relevant (reviewed in ref 1).[1] NO binding to manganese-substituted heme provides a possible scenario in which the strong Mn−NO bond formed between NO and Mn^{II} will effectively mimic the labile Fe−NO bond formed between NO and ferric Fe^{III} ion (which is isoelectronic with Mn^{II}). Indeed, MnNO derivatives of the heme biomolecules hemoglobin,[2−5] myoglobin,[6] soluble guanylyl cyclase,[7] cytochrome P450,[8] cytochrome *c*,[9,10] and cytochrome *c* peroxidase[2] have been reported. Some water-soluble manganese porphyrins are also reported to catalyze, electrochemically, the reduction of NO to hydroxylamine and ammonia in aqueous media.[11]

We recently reported the synthesis and structural characterization of a series of six-coordinate (por)Mn(NO)(L) compounds (por = tetratolylporphyrin dianion (TTP) or tetra-*p*-methoxyphenylporphyrin dianion (T(*p*-OMe)PP)); L = piperidine, 1-methyimidazole, methanol).[12] Our study complemented previous structural studies by Scheidt and coworkers[13,14] on the five-coordinate (TTP)Mn(NO) and the six-coordinate (TPP)Mn(NO)(4-Mepip) (TPP = tetraphen-

* To whom correspondence should be addressed. E-mail: grichteraddo@ou.edu.
[†] University of Oklahoma.
[‡] Southern Illinois University, Edwardsville.

(1) Cheng, L.; Richter-Addo, G. B. Binding and Activation of Nitric Oxide by Metalloporphyrins and Heme. In *The Porphyrin Handbook*; Guilard, R., Smith, K., Kadish, K. M., Eds.; Academic Press: New York, 2000; Vol. 4, Chapter 33.
(2) Yonetani, T.; Yamamoto, H.; Erman, J. E.; J. S. Leigh, J.; Reed, G. H. *J. Biol. Chem.* **1972**, *247*, 2447−2455.
(3) Gibson, Q. H.; Hoffman, B. M. *J. Biol. Chem.* **1979**, *254*, 4691−4697.
(4) Lin, S.-H.; Yu, N.-T.; Gersonde, K. *FEBS Lett.* **1988**, *229*, 367−371.
(5) Przywarska-Boniecka, H.; Swirska, H. *J. Inorg. Biochem.* **1980**, *13*, 283−296.
(6) Masuya, F.; Hori, H. *Biochim. Biophys. Acta* **1993**, *1203*, 99−103.
(7) Dierks, E. A.; Hu, S.; Vogel, K. M.; Yu, A. E.; Spiro, T. G.; Burstyn, J. N. *J. Am. Chem. Soc.* **1997**, *119*, 7316−7323.
(8) Gelb, M. H.; Toscano, W. A., Jr.; Sligar, S. G. *Proc. Natl. Acad. Sci. U.S.A.* **1982**, *79*, 5758−5762.
(9) Dickinson, L. C.; Chien, J. C. W. *J. Biol. Chem.* **1977**, *252*, 6156−6162.
(10) Przywarska-Boniecka, H.; Ostropolska, L. *J. Inorg. Biochem.* **1983**, *19*, 119−127.
(11) Yu, C.-H.; Su, Y. O. *J. Electroanal. Chem.* **1994**, *368*, 323−327.
(12) Zahran, Z. N.; Lee, J.; Alguindigue, S. S.; Khan, M. A.; Richter-Addo, G. B. *Dalton Trans.* **2004**, 44−50.
(13) Scheidt, W. R.; Hatano, K.; Rupprecht, G. A.; Piciulo, P. L. *Inorg. Chem.* **1979**, *18*, 292−299.

10.1021/ic051190n CCC: $33.50
Published on Web 02/16/2006

ylporphyrinato dianion) compounds. Other MnNO porphyrins and related derivatives have been reported and characterized spectroscopically.[1]

We were interested in examining the redox properties of the six-coordinate (por)Mn(NO)(1-MeIm) compounds containing the axial imidazole group. To the best of our knowledge, only one other electrochemical study of MnNO porphyrins has been reported, that of the five-coordinate (TPP)Mn(NO).[15] The electrochemistry of non-NO-containing manganese porphyrins is well developed.[16−18]

In this paper, we report the redox behavior of three (por)-Mn(NO)(1-MeIm) (por = TPP, TTP, T(*p*-OMe)PP)) compounds in CH_2Cl_2 and THF as determined by cyclic voltammetry, infrared spectroelectrochemistry, and bulk electrolysis.

Experimental Section

Chemicals. (TPP)Mn(1-MeIm) was prepared by the literature method.[19] Piperidine (99.5+%), 1-methyimidazole (1-MeIm, 99+%), anhydrous CH_3OH (99.8%), and tetra-*n*-butylammonium hexafluorophosphate (NBu_4PF_6) were purchased from Aldrich Chemical Co. and used as received. Chloroform-*d* (99.8%) was obtained from Cambridge Isotope Laboratories. Nitric oxide (98%, Matheson Gas) for the synthesis work was passed through KOH pellets and two cold traps (dry ice/acetone, −78 °C) to remove higher nitrogen oxides. The toluene, CH_2Cl_2, and THF solvents were distilled from calcium hydride under a nitrogen atmosphere just prior to use. Nitrogen of ultrahigh-purity grade was purchased from Trigas (Houston, TX).

The (por)Mn(NO)(1-MeIm) compounds (por = TTP, T(*p*-OMe)-PP) were prepared as previously described.[12] The red (TPP)Mn-(NO)(1-MeIm) compound was prepared in 80% isolated yield by similar procedures. IR (KBr, cm^{-1}): υ_{NO} = 1737s; also 3122vw, 3030vw, 2994vw, 2952vw, 2930vw, 2900vw, 2865vw, 1686vw, 1655vw, 1637vw, 1596w, 1533w, 1489vw, 1440w, 1420vw, 1365vw, 1348s, 1284vw, 1231w, 1204w, 1176w, 1070s, 1003s, 796s, 752s, 703s, 663w, 614vw, 526vw, 453vw. ^{1}H NMR ($CDCl_3$; δ, ppm): 8.67 (s, 8H, pyrrole-H of TPP), 8.20 (d, J = 7 Hz, 4H, *o*-H of TPP), 8.01 (d, J = 8 Hz, 4H, *o*′-H of TPP), 7.68−7.64 (overlapping m, *m*-H and *p*-H of TPP). The peaks of the 1-MeIm ligand were not observed in the spectrum at room temperature. ESI mass spectrum: *m*/*z* 667.17 $[(TPP)Mn]^+$ (68.8%), 749.2 $[(TPP)-Mn(1\text{-MeIm})]^+$ (100%). The (por)Mn(NO)(1-MeIm) complexes are stable in the solid state in air for at least 1 week (as judged by IR and ^{1}H NMR spectroscopy).

X-ray Structure Determination of (TPP)Mn(NO)(1-MeIm). Suitable crystals for X-ray crystallography were grown by slow evaporation of a CH_2Cl_2/toluene (2:1) solution of the compound containing 1-MeIm at room temperature under inert atmosphere. X-ray data were collected at 120(2) K on a Bruker Apex diffractometer (Bruker AXS, Madison, WI) using Mo Kα (λ = 0.71073 Å) radiation. Intensity data, which approximately covered the full sphere of the reciprocal space, were measured as a series of ω oscillation frames each 0.3° for 21 s/frame. The detector was operated in 512 × 512 mode and was positioned 6.12 cm from the crystal. Coverage of unique data was 94.5% complete to 53.0°-(2θ). Cell parameters were determined from a nonlinear least-squares fit of 6715 reflections in the range of 2.5 < θ < 28.2°. A total of 30 030 reflections were measured. The structure was solved by the direct method using the SHELXTL system (Version 6.12, Bruker AXS) and refined by full-matrix least squares on F^2 using all reflections. All the non-hydrogen atoms were refined anisotropically. All the hydrogen atoms were included with idealized parameters. The asymmetric unit contains one $C_{48}H_{34}MnN_7O$ molecule and 2.5 toluene solvent molecules which sit on the crystallographic 2-fold axis. The final R1 = 0.0448 is based on 10 214 "observed reflections" [$I > 2\sigma(I)$]. Details of the crystal data and structure refinement are given in Table 1. Thermal ellipsoids are drawn at 50% (Figure 1a) and 35% (Figure 1b) levels.

Table 1. Crystal Data and Structure Refinement of (TPP)Mn(NO)(1-MeIm)·2.5(toluene)

formula	$C_{65.50}H_{53.50}N_7OMn$
fw	1009.59
T (K)	120(2)
cryst syst	triclinic
space group	$P\bar{1}$
a (Å), α (deg)	9.8071(7), 105.277(1)
b (Å), β (deg)	13.0989(9), 97.316(1)
c (Å), γ (deg)	21.4652(15), 98.166(1)
V (Å^3), Z	2593.6(3), 2
D(calcd), g/cm^3	1.293
abs coeff, mm^{-1}	0.307
F(000)	1057
cryst size (mm^3)	0.28 × 0.12 × 0.04
θ range for data collection	1.66−28.26°
index ranges	$-13 \le h \le 12$, $-17 \le k \le 17$, $-28 \le l \le 27$
reflns collected	30 030
independent reflns	12 135 [R_{int} = 0.0195]
max. and min. transmission	0.9878 and 0.9191
data/restraints/params	12135/0/680
GOF on F^2	1.053
final R indices [$I > 2\sigma(I)$]	R1 = 0.0448, wR2 = 0.1202
R indices (all data)	R1 = 0.0550, wR2 = 0.1303
largest diff. peak and hole, e Å^{-3}	1.099 and −0.426

The X-ray crystal structure data have been deposited with the Cambridge Crystallographic Data Center, with reference code CCDC 278504. These data can be obtained free of charge via www.ccdc.cam.ac.uk/data_request/cif, by e-mailing data_request@ccdc.cam.ac.uk, or by contacting The Cambridge Crystallographic Data Centre, 12, Union Road, Cambridge CB2 1EZ, UK; fax: +44 1223 336033.

Instrumentation. Electrochemical measurements were performed with a BAS CV-50W instrument. IR spectra were recorded with a Bruker Vector 22 FTIR spectrometer equipped with a mid-IR fiber-optic dip probe and a liquid-nitrogen-cooled MCT detector (RemSpec corporation, Sturbride, MA). The stainless steel mirror of the fiber-optic dip probe was replaced by a Pt disk (3 mm diameter) working electrode (Bioanalytical Systems). The spectrometer was set to 4 cm^{-1} resolution. Typically 16 scans from 2200 to 1000 cm^{-1} were recorded. The IR spectroelectrochemical measurements were performed in a three-electrode cell as described previously (Pt working and auxiliary electrodes, Ag wire quasi-reference electrode).[20] The room temperature was 23 ± 1 °C. We jacketed the cell to allow for a dry ice−acetone bath (−78 °C) for

(14) Piciulo, P. L.; Rupprecht, G.; Scheidt, W. R. *J. Am. Chem. Soc.* **1974**, *96*, 5293−5295.
(15) Kelly, S.; Lançon, D.; Kadish, K. M. *Inorg. Chem.* **1984**, *23*, 1451−1458.
(16) Mu, X. H.; Schultz, F. A. *Inorg. Chem.* **1995**, *34*, 3835−3837.
(17) Kelly, S. L.; Kadish, K. M. *Inorg. Chem.* **1982**, *21*, 3631−3639.
(18) Kadish, K. M.; Van Caemelbecke, E.; Royal, G. Electrochemistry of Metalloporphyrins in Nonaqueous Media. In *The Porphyrin Handbook*; Kadish, K. M., Smith, K. M., Guilard, R., Eds.; Academic Press: San Diego, CA, 2000; Vol. 8, Chapter 55.
(19) Kirner, J. F.; Reed, C. A.; Scheidt, W. R. *J. Am. Chem. Soc.* **1977**, *99*, 2557−2563.
(20) Shaw, M. J.; Henson, R. L.; Houk, S. E.; Westhoff, J. W.; Jones, M. W.; Richter-Addo, G. B. *J. Electroanal. Chem.* **2002**, *534*, 47−53.

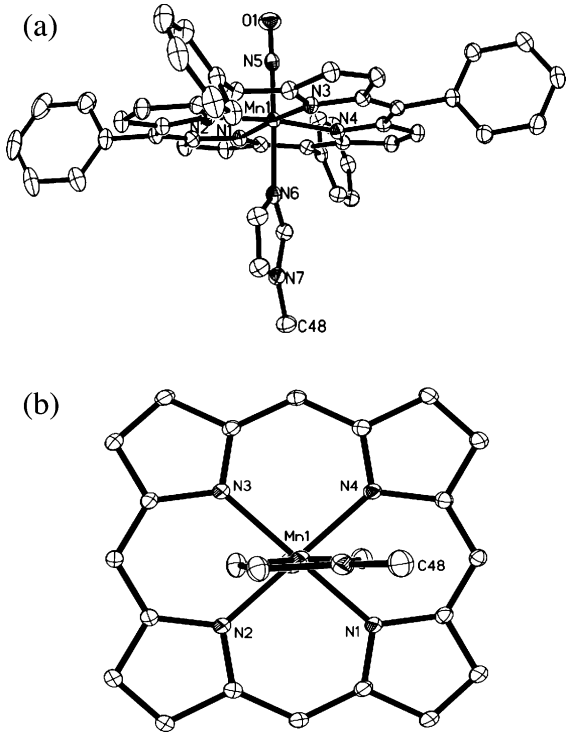

Figure 1. (a) Molecular structure of (TPP)Mn(NO)(1-MeIm). Hydrogen atoms have been omitted for clarity. (b) View of the orientation of the 1-MeIm ligand relative to the porphyrin skeleton. The porphyrin phenyl substituents have been omitted for clarity. Selected bond lengths (Å) and angles (deg) Mn−N(1) = 2.025(1), Mn−N(2) = 2.020(1), Mn−N(3) = 2.028(1), Mn−N(4) = 2.019(1), Mn−N(5) = 1.641(1), Mn−N(6) = 2.088(1), N(5)−O(1) = 1.172(2), Mn−N(5)−O(1) = 178.4(1), N(1)−Mn−N(6)−C(47) = 45.4(1) (torsion).

the low-temperature measurements. Potentials are reported versus the ferrocene−ferrocenium couple (∼ +0.46 V vs SCE).[21] Corrections for *iR* drop between the working and reference electrodes were applied. The solutions used were 0.5−1.0 mM in analyte in 10 mL of 0.1 M NBu_4PF_6. Nitrogen gas was bubbled through the solution for about 8 min before each set of measurements and was passed continuously over the surface of the solution during the measurements. Each measurement was performed in triplicate or greater.

Results

Two of the three compounds studied here have been prepared and characterized previously.[12] The third compound, namely (TPP)Mn(NO)(1-MeIm) has been prepared in 80% isolated yield. All three compounds belong to the class of {MnNO}^{6} species according to the formalism of Enemark and Feltham.[22−24] The molecular structure of (TPP)Mn(NO)(1-MeIm) is shown in Figure 1, and it reveals that the compound contains a linear MnNO moiety (∠MnNO = 178.4(1)°) and a 1-MeIm ligand trans to NO. The Mn−NO and N−O bond lengths are 1.641(1) and 1.172(2) Å, respectively. Selected structural data are shown in the caption

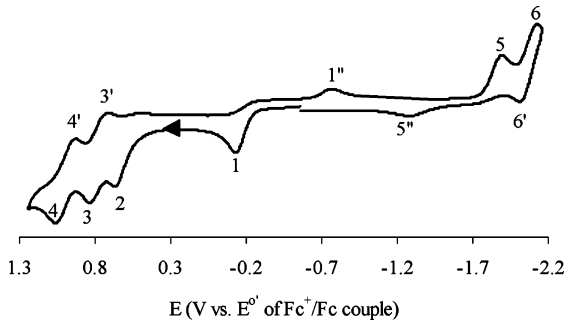

Figure 2. Cyclic voltammogram of (T(*p*-OMe)PP)Mn(NO)(1-MeIm) in CH_2Cl_2 at 23 °C. Conditions: 1 mM analyte, 100 mV/s, 0.1 M NBu_4PF_6.

of Figure 1. The structure is similar to those of the other two (por)Mn(NO)(1-MeIm) compounds (por = TTP, T(*p*-OMe)PP) whose crystal structures have been determined previously.[12]

We have examined the electrochemical properties of the (por)Mn(NO)(1-MeIm) compounds at a platinum disk electrode in a typically noncoordinating solvent (CH_2Cl_2) and in a coordinating solvent (THF). The electrochemical properties for the three compounds are similar within a given set of conditions of solvent and temperature. The data for (T(*p*-OMe)PP)Mn(NO)(1-MeIm) will be described as a representative example. We will consider oxidation processes first, followed by the reduction processes.

Oxidations. The cyclic voltammogram of (T(*p*-OMe)PP)Mn(NO)(1-MeIm) at 100 mV/s in CH_2Cl_2/0.1 M NBu_4PF_6 is shown in Figure 2. The compound exhibits a chemically irreversible oxidation at $E_{pa}(1) = -0.15$ V (peak 1 in Figure 2) vs the ferrocene−ferrocenium couple as an internal standard, and this oxidation has associated with it a small return reduction peak at −0.85 V (peak 1″) coupled with an anodic peak in a chemically reversible manner (not shown). The analysis of the data for the second oxidation ($E_{pa}(2) =$ 0.66 V; peak 2) suggests that this process consists of a slow one-electron transfer followed by a rapid irreversible chemical reaction (see later). The third and fourth oxidations, represented by couples 3/3′ ($E°'(3) = 0.78$ V) and 4/4′ ($E°'(4) = 1.05$ V) respectively, were chemically reversible. In all cyclic voltammograms shown, the primed numbers (e.g., 3′) refer to the associated return peaks in reversible processes, whereas the double-primed numbers (e.g., 1″) refer to peaks associated with products from follow-up chemical reactions.

The first oxidation process is chemically irreversible even at higher scan rates up to 1.6 V/s; an analysis of the cyclic voltammograms as a function of scan rate and the geometry of the peak ($|E_{pa}(1) - E_{pa/2}(1)| = 60 \pm 10$ mV) suggests an electrochemically reversible one-electron transfer followed by a fast irreversible chemical reaction (E_rC_i; see later). To investigate the first oxidation process further, fiber-optic IR-potential step experiments were performed at room temperature where the electrode was held at the potential corresponding to the first oxidation peak for 70 s while FTIR spectra were collected, and a cyclic voltammogram was recorded immediately after this period. The difference IR spectrum, where the unoxidized (T(*p*-OMe)PP)Mn(NO)(1-

(21) Connelly, N. G.; Geiger, W. E. *Chem. Rev.* **1996**, *96*, 877−910.
(22) Enemark, J. H.; Feltham, R. D. *Coord. Chem. Rev.* **1974**, *13*, 339−406.
(23) Feltham, R. D.; Enemark, J. H. *Top. Stereochem.* **1981**, *12*, 155−215.
(24) Westcott, B. L.; Enemark, J. H. In *Inorganic Electronic Structure and Spectroscopy*; Lever, A. B. P., Solomon, E. I., Eds.; Wiley and Sons: New York, 1999; Vol. 2 (Applications and Case Studies).

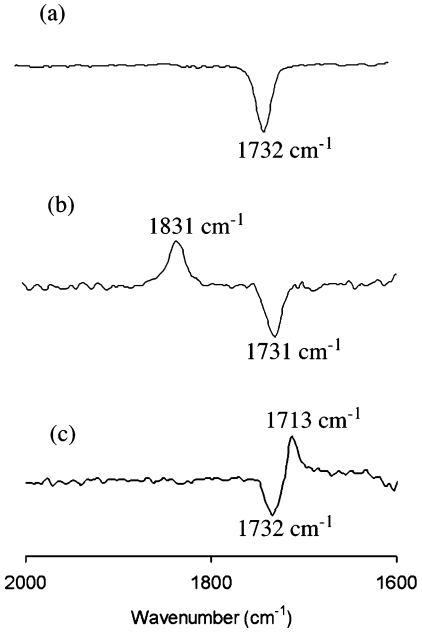

Figure 3. Difference IR spectra of (T(*p*-OMe)PP)Mn(NO)(1-MeIm) and its products in CH_2Cl_2: (a) showing the consumption of starting (T(*p*-OMe)-PP)Mn(NO)(1-MeIm) after the first oxidation without the formation of a new nitrosyl-containing species at 23 °C, (b) showing the consumption of starting (T(*p*-OMe)PP)Mn(NO)(1-MeIm) after the first oxidation with the concomitant formation of a new nitrosyl-containing species at −78 °C, and (c) showing the consumption of starting (T(*p*-OMe)PP)Mn(NO)(1-MeIm) and the formation of a new nitrosyl-containing species when the electrode potential is held at half of the peak reduction potential at 23 °C.

MeIm) was used as the background/reference is shown in Figure 3a. The data reveal a consumption of starting (T(*p*-OMe)PP)Mn(NO)(1-MeIm) near the electrode surface after the first oxidation, indicated by the loss of the NO stretching frequency at 1732 cm^{-1} (i.e., the negative peak in Figure 3a) without formation of a new nitrosyl-containing species. Bulk electrolysis at the first oxidation potential was performed on (T(*p*-OMe)PP)Mn(NO)(1-MeIm), and IR and UV−vis spectra were collected during the electrolysis experiment (panels a and b of Figures 4, respectively). Coulombic integration of one Faraday equivalent was obtained from the experiment for the first oxidation process. The IR spectra in Figure 4a show the loss of NO from the compound (similar to that observed in Figure 3a), and the UV−vis spectra show the conversion to a Mn^{III} species;[17,25] the initial Soret band at $\lambda = 429$ nm is converted into two split broad bands at 384 and 411 nm, and the Q-band at 481 nm remains at the same position but becomes more intense. This implies that the first oxidation results in a net formal oxidation at the metal center at the time scale of the bulk electrolysis with concomitant loss of NO, similar to that observed for (TPP)Mn(NO).[15]

The low temperature (−78 °C) cyclic voltammogram of (T(*p*-OMe)PP)Mn(NO)(1-MeIm) in CH_2Cl_2 is shown in Figure 5, and it shows that the first oxidation process becomes *chemically* reversible ($E^{o\prime}(1) = -0.19$ V) at low temperature. The difference IR spectra obtained after the first oxidation is shown in Figure 3b (see Discussion). The other chemically reversible oxidation peaks, at $E^{o\prime}(7) = 0.57$ V

(25) Boucher, L. J. *J. Am. Chem. Soc.* **1970**, *92*, 2725−2730.

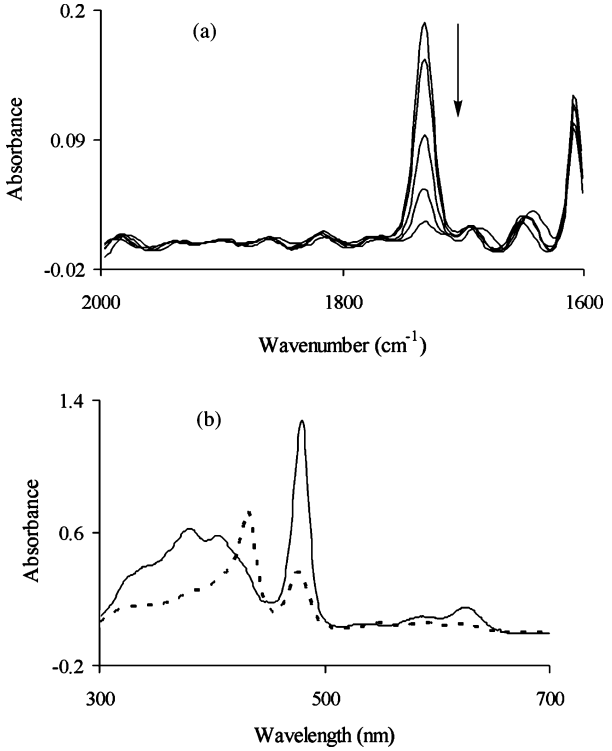

Figure 4. Infrared (a) and UV−visible (b) spectra recorded during the bulk electrolysis (first oxidation) of (T(*p*-OMe)PP)Mn(NO)(1-MeIm) in CH_2Cl_2. Conditions: 1 mM analyte, 0.29 V, 0.1 M NBu_4PF_6. The dotted line in (b) represents the spectrum of starting (T(*p*-OMe)PP)Mn(NO)-(1-MeIm).

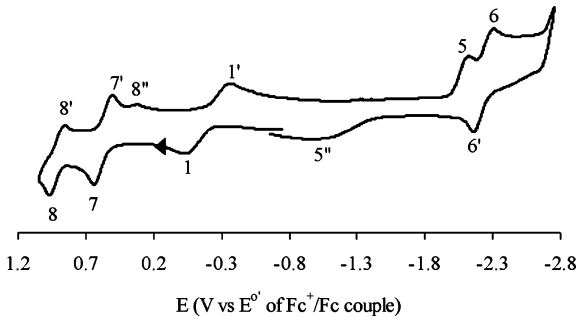

Figure 5. Cyclic voltammogram of (T(*p*-OMe)PP)Mn(NO)(1-MeIm) in CH_2Cl_2 at −78 °C. Conditions: 1 mM analyte, 100 mV/s, 0.1 M NBu_4PF_6.

(couple 7/7′) and $E^{o\prime}(8) = 0.91$ V (couple 8/8′), are attributed to further oxidation of this cationic species at low temperature.

The cyclic voltammogram of (T(*p*-OMe)PP)Mn(NO)-(1-MeIm) in the coordinating solvent THF is shown in Figure 6. The compound exhibits an irreversible oxidation (peak 1; $E_{pa}(1) = -0.05$ V) in this solvent, similar to that seen in CH_2Cl_2. Monitoring the first oxidation in THF by IR spectroelectrochemistry reveals the loss of the NO band at 1739 cm^{-1} of (T(*p*-OMe)PP)Mn(NO)(1-MeIm) without build-up of a new NO-containing species (similar to that observed in Figure 3a). There is no significant difference in the electrochemistry of (T(*p*-OMe)PP)Mn(NO)(1-MeIm) in THF at −78 and 23 °C.

Tables 2−4 summarize the electrochemical data for the three (por)Mn(NO)(1-MeIm) compounds in both solvents.

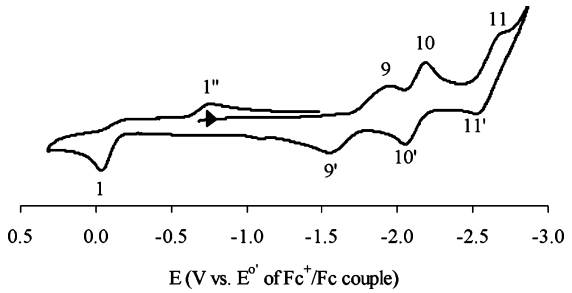

Figure 6. Cyclic voltammogram of (T(*p*-OMe)PP)Mn(NO)(1-MeIm) in THF at 23 °C. Conditions: 1 mM analyte, 100 mV/s, 0.1 M NBu_4PF_6.

Table 2. Infrared (cm^{-1}) and Electrochemical Data for the (por)Mn(NO)(1-MeIm) Compounds in CH_2Cl_2 at 23 °C[a]

		oxidations				reductions	
por	υ_{NO}	$E_{pa}(1)$	$E_{pa}(2)$	$E°'(3)$	$E°'(4)$	$E_{pc}(5)$	$E°'(6)$
TPP	1735	−0.12	0.70	0.89	1.10	−1.93	−2.11
TTP	1731	−0.15	0.69	0.83	1.05	−1.95	−2.05
T(*p*-OMe)PP	1732	−0.15	0.66	0.78	1.05	−1.94	−2.02

[a] Potentials are in volts and are referenced to the ferrocene−ferrocenium couple set at 0.00 V. Conditions: 1 mM analyte, 100 mV/s, 0.1 M NBu_4PF_6.

Table 3. Electrochemical Data for the (por)Mn(NO)(1-MeIm) Compounds in CH_2Cl_2 at −78 °C[a]

	oxidations			reductions	
por	$E°'(1)$	$E°'(7)$	$E°'(8)$	$E_{pc}(5)$	$E°'(6)$
TPP	−0.15	0.94	1.22	−2.24	−2.32
TTP	−0.16	0.74	1.10	−2.20	−2.26
T(*p*-OMe)PP	−0.19	0.57	0.91	−2.15	−2.20

[a] Potentials are in volts and are referenced to the ferrocene−ferrocenium couple set at 0.00 V. Conditions: 1 mM analyte, 100 mV/s, 0.1 M NBu_4PF_6.

Table 4. Infrared (cm^{-1}) and Electrochemical Data for the (por)Mn(NO)(1-MeIm) Compounds in THF at 23 °C[a]

		oxidation	reductions		
por	υ_{NO}	$E_{pa}(1)$	$E_{pc}(9)$	$E°'(10)$	$E°'(11)$
TPP	1741	−0.01	−1.74	−2.11	−2.59
TTP	1740	−0.03	−1.73	−2.10	−2.59
T(*p*-OMe)PP	1739	−0.05	−1.74	−2.12	−2.60

[a] Potentials are in volts and are referenced to the ferrocene−ferrocenium couple set at 0.00 V. Conditions: 1 mM analyte, 100 mV/s, 0.1 M NBu_4PF_6.

Reductions. The reduction behavior of the (por)Mn(NO)(1-MeIm) compounds at low temperature were not different from those observed at room temperature. The cyclic voltammogram of (T(*p*-OMe)PP)Mn(NO)(1-MeIm) in CH_2Cl_2 displays a chemically irreversible peak at −1.94 V (peak 5 in Figure 2) that has with it an associated small return peak at −1.25 V (labeled 5″ in the Figure). The ratio $i_{Pc}(5)/\upsilon^{1/2}$ increased linearly with increase in scan rate. In addition, the peak geometry $|E_{pc}(5) - E_{pc1/2}(5)|$ remained essentially constant at 62 mV over the potential scan range 50−1000 mV/s.

The product of the first reduction of (T(*p*-OMe)PP)Mn(NO)(1-MeIm) was examined by IR spectroelectrochemistry. Figure 3c shows the difference IR spectrum when the electrode was held at the midpoint potential $E_{pc/2}$ (5). The spectrum shows the presence of a new band that is shifted to a lower wavenumber by 19 cm^{-1}, assigned to the υ_{NO} of the monoanion $[(T(p\text{-OMe})PP)Mn(NO)(1\text{-MeIm})]^-$ (there is a slow loss of NO at this potential, however). The other two (por)Mn(NO)(1-MeIm) compounds display similar υ_{NO} shifts ($\Delta\upsilon_{NO}$ = 22 cm^{-1} for TPP and 21 cm^{-1} for TTP).

In THF, the compound shows a chemically reversible reduction with slow electron-transfer kinetics (Figure 6, peak 9; with an associated peak 9′), and two chemically reversible reductions (couples 10/10′ and 11/11′) on the cyclic voltammetry time scale.

Discussion

As mentioned earlier, the electrochemical properties of the three (por)Mn(NO)(1-MeIm) complexes are similar. Hence, the more general "por" macrocycle will be used in the equations described below. The cyclic voltammogram of (T(*p*-OMe)PP)Mn(NO)(1-MeIm) in $CH_2Cl_2/[Bu_4N]PF_6$ is shown in Figure 2, and the cyclic voltammograms of the (por)Mn(NO)(1-MeIm) compounds reveal an interesting comparison with that of (TPP)Mn(NO) in $CH_2Cl_2/[Bu_4N]ClO_4$ reported earlier by Kadish and co-workers.[15]

Oxidations. The first oxidation of (T(*p*-OMe)PP)Mn(NO)(1-MeIm) is irreversible, and the data analysis indicates an E_rC_i mechanism for the first oxidation. This mechanism is similar to that determined for (TPP)Mn(NO),[15] in which NO dissociation has been shown to occur after the first oxidation process. The first oxidation of the related (TPP)Mn(NO)(1-MeIm) compound (−0.12 V; Table 2) occurs at a more negative potential than that required for the first oxidation of the five-coordinate (TPP)Mn(NO) (−0.01 V vs Fc), and this is due to the destabilization of the Mn(II) formal oxidation state relative to the Mn(III) state in the six-coordinate (por)Mn(NO)(1-MeIm) compounds.

Our IR spectroelectrochemical studies (Figure 3a) are consistent with the loss of the NO ligand after the first oxidation of (T(*p*-OMe)PP)Mn(NO)(1-MeIm) without formation of a new NO-containing species. Thus, we assign the first oxidation to the E_rC_i process described by eqs 1 and 2.

$$(por)Mn(NO)(1\text{-MeIm}) - e^- \rightleftharpoons [(por)Mn(NO)(1\text{-MeIm})]^+ \quad (1)$$

$$[(por)Mn(NO)(1\text{-MeIm})]^+ \rightarrow [(por)Mn^{III}(1\text{-MeIm})]^+ + NO \quad (2)$$

Adding a sample of the known compound (TPP)Mn(1-MeIm)[19,26] to the solution of (TPP)Mn(NO)(1-MeIm) during the cyclic voltammetry experiments resulted in an increase in the intensity of the redox couple at $E°'$ = −0.77 V associated with the analogous 1″ peak in Figure 2 (i.e., eq 3), as expected if $[(por)Mn(1\text{-MeIm})]^+$ was indeed produced from eq 2. This Mn(III)/Mn(II) couple at −0.77 V (eq 3) is similar to the Mn(III)/Mn(II) couple determined for (TPP)MnCl in $CH_2Cl_2/[Bu_4N]BF_4$ (−0.81 V),[27] and in $CH_2Cl_2/[Bu_4N]ClO_4$ (−0.78 V).[15]

(26) Gonzalez, B.; Kouba, J.; Yee, S.; Reed, C. A.; Kirner, J. F.; Scheidt, W. R. *J. Am. Chem. Soc.* **1975**, *97*, 3247−3249.
(27) Foran, G. J.; Armstrong, R. S.; Crossley, M. J.; Lay, P. A. *Inorg. Chem.* **1992**, *31*, 1463−1470.

$$[(\text{por})\text{Mn}^{\text{III}}(\text{1-MeIm})]^+ + e^- \rightleftharpoons (\text{por})\text{Mn}^{\text{II}}(\text{1-MeIm}) \quad (3)$$

The intensities of the peaks in Figure 2 associated with the second (peak 2), third (couple 3/3′), and fourth (couple 4/4′) oxidations also increased as well, suggesting that these further oxidations are due to electrogenerated [(por)Mn(1-MeIm)]$^+$ or its products.

The irreversibility of peak 2 in Figure 2 suggests a loss of the axial 1-MeIm ligand after this second oxidation (eqs 4 and 5).

$$[(\text{por})\text{Mn}^{\text{III}}(\text{1-MeIm})]^+ - e^- \rightleftharpoons [(\text{por})\text{Mn}^{\text{III}}(\text{1-MeIm})]^{2+} \quad (4)$$

$$[(\text{por})\text{Mn}^{\text{III}}(\text{1-MeIm})]^{2+} \rightarrow [(\text{por})\text{Mn}^{\text{III}}]^{2+} + \text{1-MeIm} \quad (5)$$

We note that the previously reported second (*reversible*) oxidation of the five-coordinate (TPP)Mn(NO) compound (presumably the reversible oxidation of electrogenerated [(TPP)Mn]$^+$) is at $E_{1/2} = 0.69$ V (vs Fc),[15] whereas the second (*irreversible*) oxidation of (TPP)Mn(NO)(1-MeIm) is at $E_{pa}(2) = 0.70$ V. This difference is not unexpected, since the products of the first oxidation of (TPP)Mn(NO) and (TPP)Mn(NO)(1-MeIm) are different. Indeed, this result is consistent with the presence of 1-MeIm in the latter compound making it easier to oxidize.

The large difference between $E_{pa}(1)$ and $E_{pa}(2)$ is not inconsistent with a change from a metal-centered oxidation ($E_{pa}(1)$) to a ring-centered oxidation ($E_{pa}(2)$). The relatively smaller difference between the second and third oxidations ($|E^{\circ\prime}(3) - E_{pa}(2)| = 0.12$ V) and the third and fourth oxidations ($|E^{\circ\prime}(4) - E^{\circ\prime}(3)| = 0.27$ V) suggests ring-centered redox processes.[18]

Rogers and Goff[28] have examined the products of chemical and electrochemical oxidation of tetraarylporphyrin manganese complexes in CH_2Cl_2 and have proposed the formation of isoporphyrins from some highly oxidized (por)MnX compounds (por = TPP, TMP; X = Cl, OAc). For example, a peak at +0.6 V vs SCE in the room-temperature cyclic voltammogram of (TPP)MnX was tentatively assigned to an isoporphyin derivative. In the presence of 4-Mepy, however, the peak assigned to the isoporphyrin was not observed.[28] We do not observe such a 0.6 V peak (0.14 V vs Fc) in our experiments involving the (por)Mn(NO)(1-MeIm) compounds on the cyclic voltammetry time scale, although we cannot rule out the formation of such species on longer experimental time scales.

We focused on the identities of the products of the first oxidation processes for the (por)Mn(NO)(1-MeIm) compounds, and we were interested in stabilizing the first oxidation products at low temperature. We have previously reported a simple infrared reflectance spectroelectrochemical setup for the study of short-lived species generated at the electrode surface.[20] We have modified the glassware slightly to allow for jacketing of the cell compartment with a dry ice bath, and we have found this practical for low-temperature infrared spectroelectrochemistry.

The cyclic voltammogram of (T(*p*-OMe)PP)Mn(NO) in CH_2Cl_2 at −78 °C is shown in Figure 5 and reveals that the product of the first oxidation (eq 1) is indeed stabilized at low temperature.

Further evidence for a stable [(por)Mn(NO)(1-MeIm)]$^+$ oxidation product from eq 1 comes from IR spectroelectrochemistry at −78 °C. The difference IR spectrum upon oxidation of (T(*p*-OMe)PP)Mn(NO)(1-MeIm) at −78 °C is shown in Figure 3b, and it reveals a new IR υ_{NO} band that is 100 cm^{-1} *higher* in energy than that of the parent compound. Such a large shift in υ_{NO} is indicative of metal−NO-centered oxidations in nitrosylmetalloporphyrins, although larger υ_{NO} shifts of 166−187 cm^{-1} have been observed upon similar electro-oxidations of some iron nitrosyl porphyrins;[29] however, these latter cases likely involve a change in geometry of the FeNO linkages from bent to linear. The other two (por)Mn(NO)(1-MeIm) compounds have similar υ_{NO} shifts ($\Delta\upsilon_{NO} = 111$ cm^{-1} for TPP, and 108 cm^{-1} for T(*p*-OMe)PP; spectra not shown) upon low-temperature oxidations in CH_2Cl_2.

Follow-up reversible redox processes are observed in the cyclic voltammogram of (T(p-OMe)PP)Mn(NO)(1-MeIm), as observed in Figure 5, and we assign these tentatively to the processes described by eqs 6 and 7.

$$[(\text{por})\text{Mn}(\text{NO})(\text{1-MeIm})]^+ - e^- \rightleftharpoons [(\text{por})\text{Mn}(\text{NO})(\text{1-MeIm})]^{2+} \quad (6)$$

$$[(\text{por})\text{Mn}(\text{NO})(\text{1-MeIm})]^{2+} - e^- \rightleftharpoons [(\text{por})\text{Mn}(\text{NO})(\text{1-MeIm})]^{3+} \quad (7)$$

The product of eq 7 is not very stable, generating a secondary species with an associated peak at 8″ in Figure 5. The large 1/1′ peak separation ($\Delta E = 315$ mV) in Figure 5 suggests slow electron-transfer kinetics for this metal-centered process, relative to the fast electron processes associated with the ring-centered 7/7′ and 8/8′ redox couples. In general, the voltammograms shown in Figures 2 and 5 are representative of the voltammograms obtained for all three (por)Mn(NO)(1-MeIm) compounds in CH_2Cl_2.

We also examined the redox behavior of the compounds in the coordinating solvent THF. The first oxidation is irreversible, and we suggest an electrochemical oxidation (eq 1) followed by loss of NO involving coordination of the solvent (eq 8).

$$[(\text{por})\text{Mn}(\text{NO})(\text{1-MeIm})]^+ + \text{THF} \rightarrow [(\text{por})\text{Mn}^{\text{III}}(\text{1-MeIm})(\text{THF})]^+ + \text{NO} \quad (8)$$

The peak at 1″ can then be represented by the reduction of the product of eq 8 (i.e., eq 9).

$$[(\text{por})\text{Mn}^{\text{III}}(\text{1-MeIm})(\text{THF})]^+ + e^- \rightleftharpoons (\text{por})\text{Mn}^{\text{II}}(\text{1-MeIm})(\text{THF}) \quad (9)$$

(28) Rodgers, K. R.; Goff, H. M. *J. Am. Chem. Soc.* **1988**, *110*, 7049−7060.

(29) Mu, X. H.; Kadish, K. M. *Inorg. Chem.* **1988**, *27*, 4720−4725.

The cyclic voltammogram is not altered when the data are recorded at −78 °C, indicating that THF coordination (eq 8) results in a significant denitrosylation of the first oxidation product.

Reductions. The data for the reduction of (T(*p*-OMe)PP)Mn(NO)(1-MeIm) in CH_2Cl_2 (peak 5 in Figure 2) are consistent with an E_rC_i mechanism (eqs 10 and 11).

$$[(\text{por})\text{Mn(NO)(1-MeIm)}] + e^- \rightleftharpoons [(\text{por})\text{Mn(NO)(1-MeIm)}]^- \quad (10)$$

$$[(\text{por})\text{Mn(NO)(1-MeIm)}]^- \rightarrow [(\text{por})\text{Mn(1-MeIm)}]^- + \text{NO} \quad (11)$$

Evidence for the existence of the short-lived [(por)Mn(NO)(1-MeIm)]$^-$ monoanion is provided by IR spectroelectrochemistry, as shown in Figure 3c. The relatively small shift in υ_{NO} ($\Delta\upsilon_{NO} = 19$ cm^{-1}) upon reduction suggests that the reduction is centered on the porphyrin ring rather than on the MnNO fragment. *The new* υ_{NO} band disappears completely at $E_{pc}(5)$ or at lower potentials, indicative of a fast rate of NO loss at $E_{pc}(5)$. The first reduction peak is coupled to a return peak at −1.25 V labeled 5″ in Figure 2. We thus assign peak 5″ to the oxidation of electrogenerated [(T(*p*-OMe)PP)Mn(1-MeIm)]$^-$ as shown in eq 12.

$$[(\text{por})\text{Mn(1-MeIm)}]^- - e^- \rightleftharpoons [(\text{por})\text{Mn}^{\text{II}}\text{(1-MeIm)}] \quad (12)$$

In the case of the previously reported five-coordinate compound (TPP)Mn(NO), the first reduction process occurs at −1.41 V[15] and is reversible. The reduction of (TPP)Mn(NO)(1-MeIm) thus occurs at a more negative potential (at −1.93 V; Table 2), a shift of −0.52 V due to the presence of the axial 1-MeIm ligand. We note that the reduction of (TPP)Mn(NO)(py) also occurs at a potential that is more negative (by −0.40 V) than that needed for (TPP)Mn(NO),[15] and it also exhibits irreversible reduction behavior. In contrast to the first reduction of (TPP)Mn(NO)(1-MeIm) in CH_2Cl_2/$[Bu_4N]PF_6$, however, the irreversible reduction of (TPP)Mn(NO)(py) in CH_2Cl_2/$[Bu_4N]ClO_4$ results in the loss of the axial py ligand rather than NO on the cyclic voltammetry time scale.

A second chemically reversible reduction in CH_2Cl_2 (represented by the 6/6′ couple in Figure 2) is thus attributed to the reduction of the electrogenerated [(por)Mn(1-MeIm)]$^-$ species.

We attribute the first reduction of (T(*p*-OMe)Mn(NO)(1-MeIm) in THF (peak 9 in Figure 6) to the process described by eq 10. However, the slow loss of NO upon reduction in THF suggests an additional process (eq 13) which may be intimately coupled with eq 10.

$$[(\text{por})\text{Mn(NO)(1-MeIm)}]^- \rightleftharpoons [(\text{por})\text{Mn(1-MeIm)(THF)}]^- + \text{NO} \quad (13)$$

The positive shift in the first reduction potential in THF (−1.74 V) compared to that in CH_2Cl_2 (−1.94 V) is indicative of solvent coordination in the product. Consistent with this is the observation that holding the potential at $E_{pc}(9)$ or at values more negative to this value results in complete loss of NO.

Scheme 1

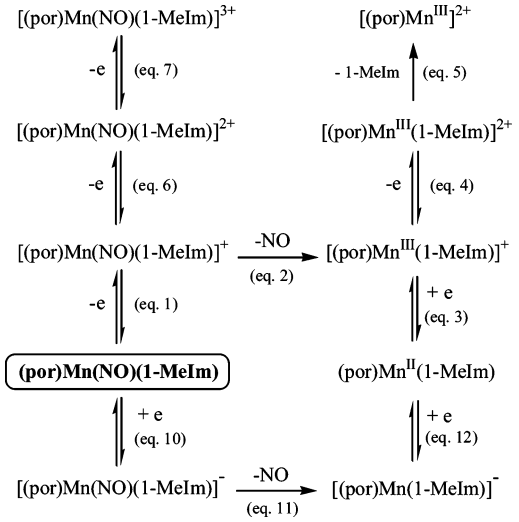

Interesting comparisons can thus be made between the electroreductions of the (por)Mn(NO)(1-MeIm) complexes and the electroreductions of the five-coordinate (TPP)Mn(NO) compound in the presence of Lewis bases. Reduction of (TPP)Mn(NO) in the mixed solvent systems CH_2Cl_2/DMF, CH_2Cl_2/Me_2SO, and CH_2Cl_2/py results in the formation of the [(TPP)Mn(NO)(S)]$^-$ anion (S = donor solvent); NO remains coordinated in the shorter time scale of cyclic voltammetry, but is dissociated at longer experimental time scales.[15] For example, in neat pyridine, the electrochemical reduction of (TPP)Mn(NO)(py) is neat and reversible and produces [(TPP)Mn(NO)(py)]$^-$.

The other two redox processes (couples 10/10′ and 11/11′) are thus due to the reductions of non-nitrosyl-containing species and are reversible.

Summary. The redox behavior of the (por)Mn(NO)(1-MeIm) compounds in CH_2Cl_2 at room temperature and at −78 °C may be summarized as shown in Scheme 1. As mentioned in the Introduction, only one other electrochemical study of manganese nitrosyl porphyrins has been reported, namely that of the five-coordinate compound (TPP)Mn(NO).[15]

The first oxidation of (por)Mn(NO)(1-MeIm) at room temperature is essentially irreversible and follows an E_rC_i mechanism resulting in the net loss of NO (eqs 1 and 2). This is similar to that reported for (TPP)Mn(NO) (i.e., denitrosylation upon oxidation), except that in the present study the product of the first oxidation is a five-coordinate [(por)Mn(1-MeIm)]$^+$ species which undergoes an irreversible oxidation (eqs 4 and 5) to lose the axial ligand. We have stabilized the product of the first oxidation (eq 1) by recording the redox behavior at −78 °C. At this temperature, the initial oxidized product [(por)Mn(NO)(1-MeIm)]$^+$ undergoes two further reversible oxidations (eqs 6 and 7).

The reduction behavior of (por)Mn(NO)(1-MeIm) is different from that of the five-coordinate (TPP)Mn(NO). In

the case of (TPP)Mn(NO),[15] this compound undergoes two successive reductions without loss of NO. For the six-coordinate (por)Mn(NO)(1-MeIm), however, denitrosylation occurs after the first reduction (eqs 10 and 11). Importantly, our infrared spectroelectrochemistry setup,[20] which we have now adapted for low-temperature work, has allowed us to identify several of the nitrosyl-containing species in the redox reactions of the six-coordinate manganese nitrosyl porphyrins (por)Mn(NO)(1-MeIm).

Acknowledgment. We thank the National Institutes of Health (GM 64476) for financial support of this work. Z.N.Z. is grateful to the Government of Egypt for a graduate fellowship.

Supporting Information Available: Crystallographic data in cif format. This material is available free of charge via the Internet at http://pubs.acs.org.

IC051190N